



## Experimental study of a novel lighting support system reinforced with a pulley friction damper

Han V. Tran <sup>a</sup>, Sung Chan Kim <sup>b</sup>, Jiuk Shin <sup>c</sup>, Kihak Lee <sup>a,\*</sup>

<sup>a</sup> Deep Learning Architecture Research Center, Department of Architectural Engineering, Sejong University, 209 Neungdong-ro, Gwangjin-gu, Seoul, 05006, Republic of Korea

<sup>b</sup> Sehong Inc, Ltd, 16, Tapsil-ro 58, Giheung-gu, Yongin-si, Gyeonggi-do, 17084, Republic of Korea

<sup>c</sup> Department of Architectural Engineering, Gyeongsang National University, Jinju-daero, Jinju-si, Gyeongsangnam-do, 52828, Republic of Korea



### ARTICLE INFO

#### Keywords:

Pulley wireway system  
Shaking table test  
Friction damper  
Non-structural components  
Vibration attenuation

### ABSTRACT

The pulley wireway system, a novel lighting support system reinforced with a pulley friction damper, can become an attractive alternative earthquake-resistant for conventional lighting system in the building. The goal of this research was to conduct a thorough evaluation of the seismic energy dissipation capacities of a novel and an existing lighting support systems under artificial earthquakes of varying magnitudes generated using the ICC-ES AC156 standard. This was achieved by conducting tri-axial shaking table tests on two specimens suspended from the same height and using the same connector type. The experimental results demonstrated that the newly developed lighting support system with the damper was effective in reducing the seismic energy and peak oscillation. The effectiveness of the damper was directly proportional to the magnitude of the earthquake, resulting in the excellent adaptability of this innovative system to a wide range of earthquake events.

### 1. Introduction

The report from the past earthquakes indicates that the non-structural components (NSCs) are susceptible to damage and failure even when the structure is subjected to low and moderate earthquakes [1], resulting in unpredictable economic losses [2,3] and impeding timely rescue of the injured. The high vulnerability of electrical systems, one type of the NSCs [4], was clearly showed at San Francisco International Airport during the 1989 Loma Prieta earthquake [5,6]; a major local hospital in Los Angeles in the 1994 Northridge earthquake [7]; vital facilities in the 1985 Mexico Earthquake and the 2010 Haiti Earthquake [4]; crucial public buildings, such as hospitals, Korea train express (KTX) railway stations in the 2016 Gyeongju and 2017 Pohang earthquakes in South Korea [8]. The paper discusses the lighting support system, which is a type of electrical systems.

To date, few studies have investigated the seismic behavior of electrical components. Hwang et al. [9] used actual earthquake damage data to conduct a seismic fragility analysis of electrical equipment in a typical electric substation in the eastern United States. Porter et al. [10] evaluated the fragility of many types of electrical equipment that are frequently found in commercial and industrial buildings. Wang et al. [11] carried out quasi-static cyclic loading tests and shaking table tests to investigate the seismic performance of a prototype diesel generator equipped with a restrained vibration isolation system. Son et al. [12] conducted experimental tests for seismic qualification of an electrical cabinet based on a shaking table. Dinh et al. [13] performed an experimental seismic investigation of a 1000 kVA cast resin-type hybrid mold transformer though a tri-axial shaking table test. Notably, none of the research addresses the

\* Corresponding author.

E-mail address: [kihaklee@sejong.ac.kr](mailto:kihaklee@sejong.ac.kr) (K. Lee).

seismic performance of the lighting support system.

Recently, Sehong Inc., Ltd. has developed a lighting support system known as the one-way system (the existing lighting structure support). The one-way system has been installed in several projects in South Korea such as Suwon SK V1 Motors, Sejong-ro Complex in Seoul, Ulsan Exhibition and Convention Center, and Bitgoeul Office in Gwangju, Jeollanam-do. Based on the design of this existing lighting structure support, the study proposes a novel lighting support system called the pulley wireway system. This system is unique in that it utilizes a pulley as a simple and effective friction damper to dissipate the seismic energy.

Tri-axial shaking table tests were carried out to evaluate the seismic performance of the proposed system and the existing system. A pulley wireway system and an existing lighting structure support with the same boundary condition were selected as the test specimens. The input acceleration time histories were artificially generated to match the requirement proposed by the International Code Council Evaluation Services Acceptance Criteria ICC-ES AC156 with a range of different amplitudes [14]. In addition, random input signals were also used for dynamic identification according to FEMA 461 [15]. Based on the test results, the damage and dynamic characteristics of the proposed system and the existing system were compared, evaluated and investigated under tri-axial acceleration, simulating an earthquake event, in terms of fundamental frequency, acceleration time history responses, maximum displacement response, system peak oscillation, and seismic energy.

## 2. Concept of the proposed pulley friction damper

### 2.1. Conceptual configuration of the pulley wireway system

**Fig. 1** shows the developed conceptual configuration of the pulley friction damper. The pulley friction damper is attached to the main structure by a bolt connection through an end base. The pulley base is joined to the end base with the help of two bolts, two nuts, and two washers. The pulley base serves as a support for the pulley. An aluminum pipe and a shaft are used to enable the pulley to rotate around a vertical axis. Additionally, the bottom end of this shaft is threaded, enabling it to connect to the bottom hole in the pulley base. A cable is rolled around the pulley to connect the damper to the lighting system.

The pulley friction damper can dissipate seismic energy by utilizing mechanical friction generated between the pulley and the pulley base, the pulley and the aluminum pipe, and the friction created between the cable and the pulley. A mechanism controls the seismic energy dissipation of the damper by a spring coaxial with the rotation axis of the pulley. The two ends of the spring are placed into one bottom washer and one top washer. The compression force exerted by the spring on the pulley controls the efficiency of the seismic energy dissipation of the damper. Compression is controlled by adjusting the length of the spring, which is adjusted by changing the positions of the top washer and the shaft. Additionally, the effectiveness of the seismic energy dissipation of the damper can be controlled by adjusting the tension of the cable by a towing machine at the opposite end of the system.

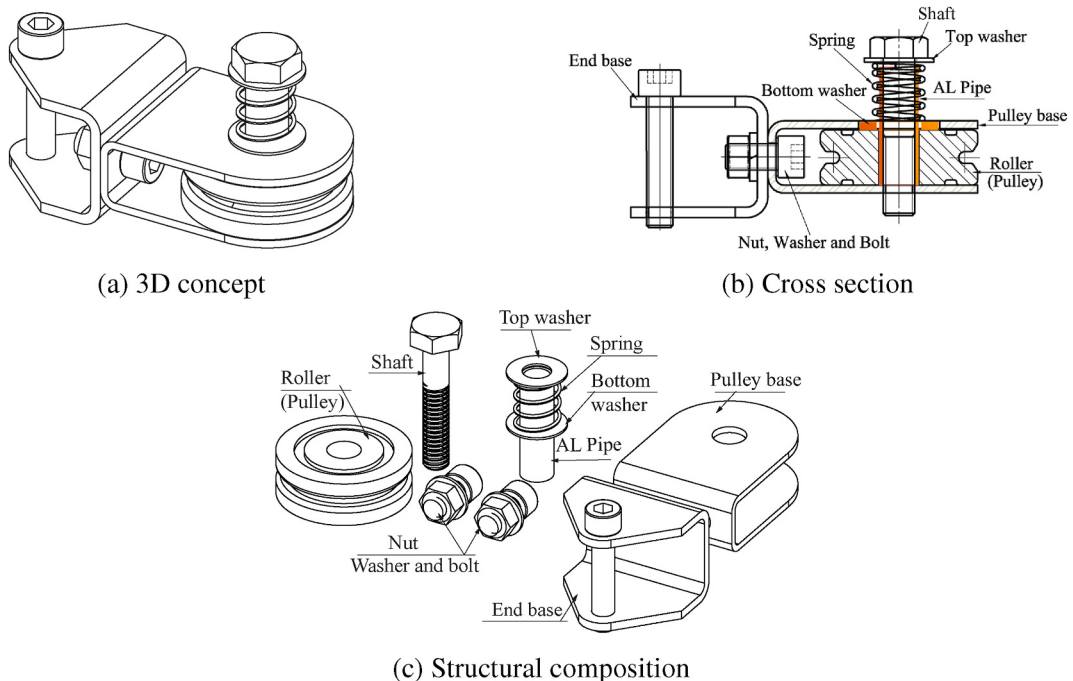


**Fig. 1.** Concept of pulley friction damper.

## 2.2. Mechanism of the pulley friction damper

### 2.2.1. Sliding mechanism of the cable and pulley

The three slip states between the pulley and cable are shown in Fig. 2: (1) nonslip state, (2) partial slip state and (3) full slip state [16]. When an earthquake acts on the lighting system, under the inertial force, the tension in the cable changes continually due to the fluctuations of the earthquake acceleration. Let  $T_2$  and  $T_1$  be the tension at the two ends of the cable ( $T_2 \geq T_1$ ), and  $\mu$  is the friction coefficient. Based on the research of Lubarda et al. [17], the contact arc  $\theta$  is divided into two parts: an active arc and an inactive arc where slip does not occur with angles of  $\theta_s$  and  $(\theta - \theta_s)$ , respectively.  $T_2^c$  is the maximum tension required of  $T_2$  to prevent the rope from fully slipping relative to the pulley [18]:

$$\frac{T_2^c}{T_1} = e^{\mu\theta} \quad (1)$$

Thus, the requirements necessary for the existence of sliding states between the pulley and the cable are as follows:

- Non slip state:  $T_2 = T_1; \theta_s = 0$
- Partial slip state:  $T_1 < T_2 < T_2^c; 0 < \theta_s = \ln\left(\frac{T_2}{T_1}\right) \frac{1}{\mu} < \theta$
- Full slip state:  $T_2 \geq T_2^c; \theta_s = \theta$

The friction force between the pulley and the cable  $F_f$  is responsible for the rotation of the pulley around its vertical axis.

### 2.2.2. Mechanism of the pulley friction damper

The three-stage working mechanism of the pulley friction damper is shown in Fig. 3, i.e.: (1) static friction stage, (2) sliding friction stage (the pulley turns clockwise) and (3) sliding friction stage (the pulley turns counterclockwise).

Assume that  $F_s$  is the compression force on the spring.  $F_{np}$  and  $F_{nbp}$  represent the normal forces exerted by the pulley on the bottom washer and the pulley base on the pulley, respectively. Let  $M_{fcp}$  be the torque generated by the friction between the pulley and the cable.  $M_{fwp}$ ,  $M_{fppi}$ , and  $M_{fppb}$  are torques generated by the friction between the top washer and pulley, the pulley and AL pipe, and the pulley and pulley base.

The pulley friction damper remains in the static friction stage when the torque of the friction force between the pulley and the cable acting on the pulley is less than the selected level of activation torque (Eq. (2)) shown in Fig. 3a. This means that the pulley does not rotate.

$$M_{fcp} \leq M_{fwp} + M_{fppi} + M_{fppb} \quad (2)$$

When the friction force between the pulley and the cable exceeds the activation torque (Eq. (3)), the pulley begins to rotate vertically. The pulley begins to slide relative to the pulley base and top washer, generating friction and dissipating energy in the process. It is either at the sliding friction stage (the pulley rotates clockwise) or the sliding friction stage (the pulley rotates counterclockwise) shown in Fig. 3b and c.

$$M_{fcp} > M_{fwp} + M_{fppi} + M_{fppb} \quad (3)$$

Consequently, the efficiency of the energy dissipation of the pulley damper can be controlled by adjusting the spring compression and initial tension at the two ends of the cable. Additionally, it is dependent on the magnitude of the earthquake that acts on the system.

## 3. Shaking table test

### 3.1. Description of the test specimens

To evaluate the capability of the existing and novel lighting system, two specimens with the same width and length of 128 and 3680 mm were fabricated. Each specimen weighed around 27 kg. The composition and installation of the two specimens are shown in

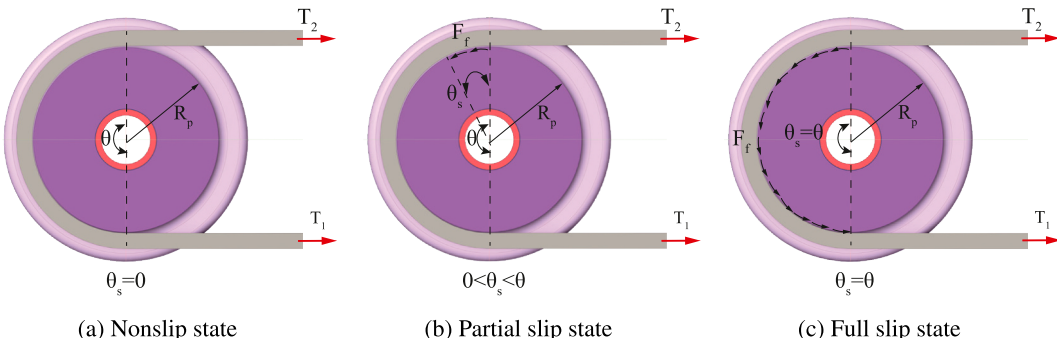


Fig. 2. Sliding state of pulley and cable.

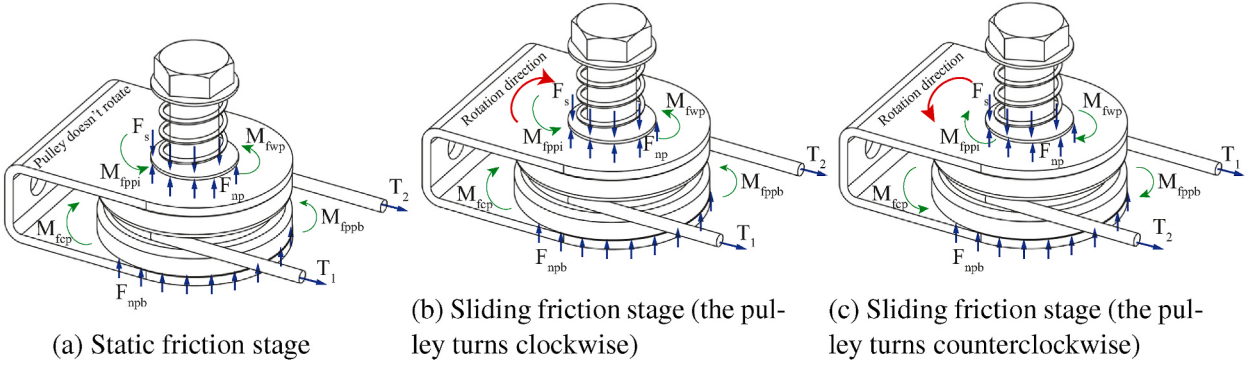


Fig. 3. Working mechanism of pulley friction damper.

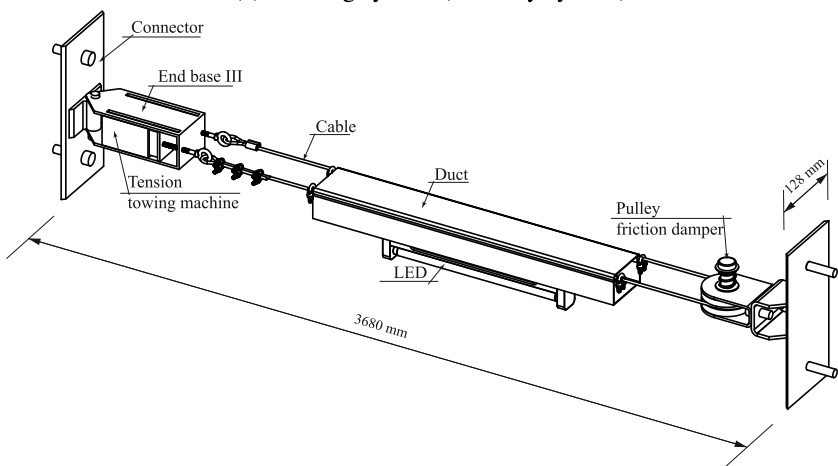
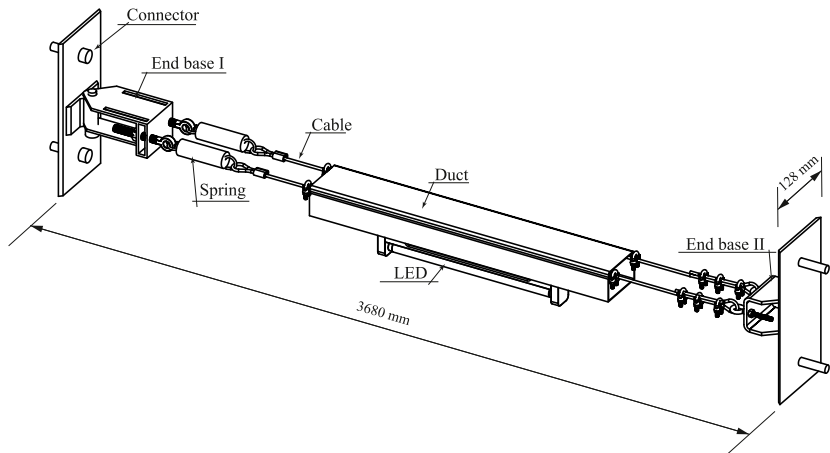


Fig. 4. Detail of the existing and pulley wireway system specimens.

**Fig. 4.**

The existing system specimen consisted of two parallel cables connected to the end base I and end base II. The cable pre-tension was generated by a spring-mounted at one end, which was used to correct sagged cable and maintain level along its length. In comparison, the pulley wireway system specimen consisted of a cable wrapped around a pulley friction damper. The diameter of the pulley is 60 mm. To manage the pre-tension between the two cable ends, a tension towing machine, which was attached to end base III, was

employed. This machine was capable of independently setting the pre-tension at each end of the cable. The tension values for each cable end were displayed on the respective side via divisions.

Before conducting the test, the pre-tension was set at 1500 N on both ends of the cable to ensure that two specimens had the same initial deflection. A 34 W LED with a 1070 mm length was suspended by cables from a 60 × 70 × 2500 mm aluminum duct. The spring of the pulley friction damper had a compression force of 120 N. Two specimens were attached to the frame using identical connectors.

Aluminized alloy of the grade AL6063 and AL6061 was used to fabricate the duct and pulley, respectively. The cable consists of stainless steel and has a diameter of 4 mm. It is a seven-strand cable with seven wires (7 × 7) and has a diameter of seven strands. The pulley base, end bases I, II and III are made of steel with the grade SS400. The connectors are steel with the grade SUS304. Mechanical parameters of the specimen components and system-wide characteristics for each portion were established by the manufacturer in accordance with Korean Standard specifications. The mechanical characteristics of the cable are presented in Table 1. Table 2 presents the material qualities of the stainless steel and aluminum alloy materials used for the remainder of the parts.

### 3.2. Test setup and measuring instruments

The experiments were carried out on a shaking table with dimensions of 4 × 4 m. The shaking table was an electro-hydraulic servo with three variable controls, six degrees of freedom (X, Y, Z, RX, RY, RZ) and 62 channels. The frequency range used was between 0.1 and 60 Hz. The payload capacity is 30000 kg.

A steel frame with two stories and one bay was utilized to replicate a single room structure inside a building for the purpose of placing the lighting structure support. The steel frame for the first floor was comprised of four steel beams and four steel columns. The steel frame for the second level was comprised of only one steel beam (T-beam) and two steel columns, which were bolted to the grid beam of the first floor.

The pulley wireway system and the existing system specimens were both attached on two steel beams of the shaking table via the same connectors. The specimens are mounted at a height of  $z = 1.07$  m from the base of the shaking table. The accelerometer A1 was placed at the base of the shaking table ( $z = 0$  m). Accelerometers A3 and A5 were installed at the top of the T-beam ( $z = 2.717$  m) and at the top of the steel column on the first floor ( $z = 1.645$  m) to record the acceleration responses at various elevation positions in the steel frame. Accelerometers A2 and A4 mounted at the top midpoint of the duct were used to record the acceleration responses of the pulley wireway and the existing system, respectively. The displacement of the pulley wireway and the existing system was recorded by the LVDT D1 and D2 that were put at the top midpoint of the duct of the two systems. Fig. 5 shows the test set-up, and the locations of the accelerometers A1–A5 and the LVDT D1–D2.

### 3.3. Input and testing protocol

A shaking table test was carried out at the Earthquake Disaster Prevention Research Center of Pusan National University, which has the capability of operating a shaking table with six degrees of freedom. The shaking table test was confirmed to investigate the seismic performance of the specimens in compliance with the seismic qualification test of specifications based on the ICC-ES AC156 [14] and SPS-F KOSED 0007-7419:2021 [19]. The used seismic input was generated to satisfy required response spectrum (RRS), which is the lowest seismic acceleration required to excite a target component as a function of the natural period or natural frequency. RRS developed from the two parameters: the story height ratio ( $z/h$ ), and the design spectral response acceleration at short periods  $S_{DS}$ , as shown in Fig. 6.

The horizontal spectral acceleration for flexible  $A_{FLX-H}$  and rigid  $A_{RIG-H}$  components are computed as follows [14]:

$$A_{FLX-H} = S_{DS} \left( 1 + 2 \frac{z}{h} \right) \leq 1.6 S_{DS} \quad (4)$$

$$A_{RIG-H} = 0.4 S_{DS} \left( 1 + 2 \frac{z}{h} \right) \quad (5)$$

The vertical spectral acceleration of the flexible  $A_{FLX-V}$  and rigid  $A_{RIG-V}$  components are computed as follows [14]:

$$A_{FLX-V} = 0.67 S_{DS} \quad (6)$$

$$A_{RIG-V} = 0.27 S_{DS} \quad (7)$$

According to several studies by Korean authors, such as Jun et al. [20], Dinh et al. [13] and Kim et al. [21], and the Korean Design Standard [22] (KCSC 2019), the value of  $S_{DS}$ , which indicates the seismic hazard of Seoul, South Korea, was 0.50 g under the

**Table 1**  
Mechanical characteristics of cable.

Item	Value	Units
Wire structure	7 × 7	–
Diameter	4	mm
Maximum load bearing	9.8	kN
Weight per unit length	0.066	kg/m
Displacement (50kgf tensile load)	0.7	mm
Modulus of elasticity	96105	MPa

**Table 2**  
Mechanical properties of the main parts of the system.

Material	Density (g/cc)	Tensile Strength (Ultimate) (MPa)	Tensile Strength (Yield) (MPa)	Elongation at Break (%)	Tensile Modulus (GPa)	Poisson's Ratio
AL6063	2.70	150	90	20	69	0.33
AL6061	2.70	310	276	12–17	68.9	0.33
SUS304	8.00	590	330	40	193	0.29
SS400	7.80	415	205	21	160	0.25

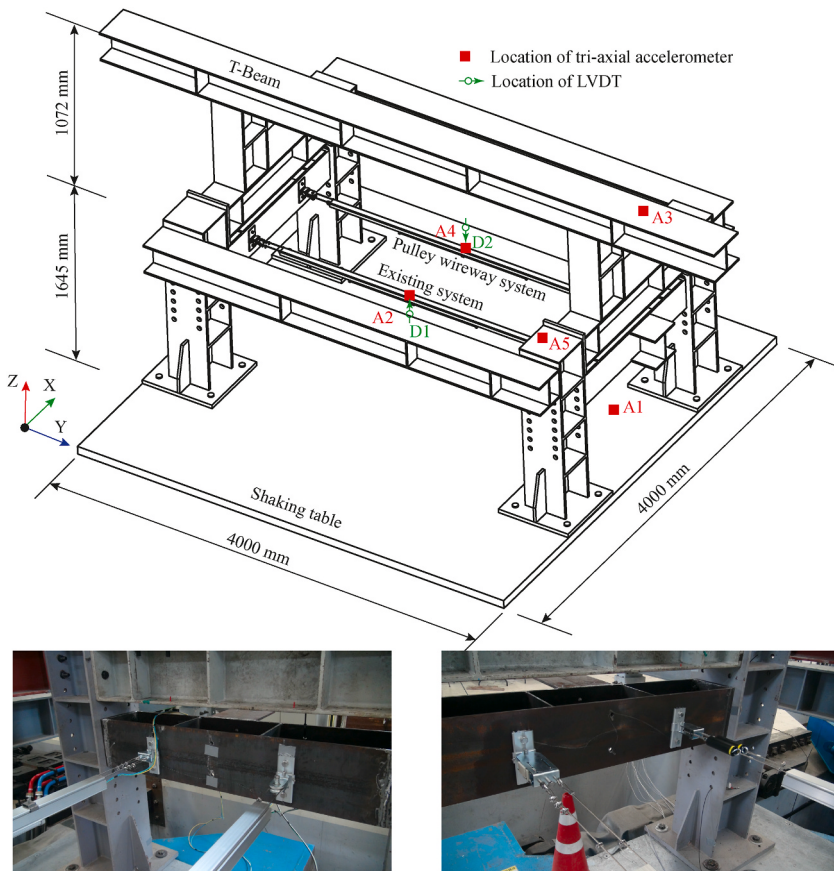


Fig. 5. Shaking table test set-up and measurement instrumentation.

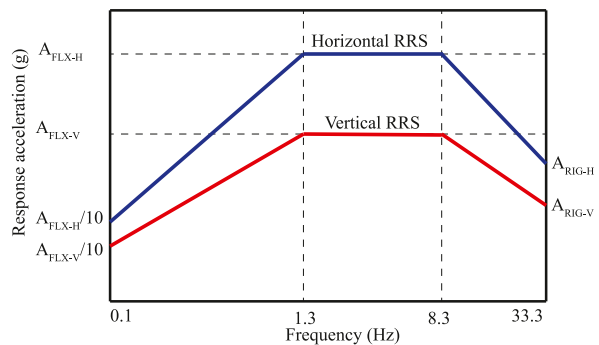


Fig. 6. Reacquire response spectrum (AC156).

assumptions of a Site Class D (stiff) soil condition. Artificial acceleration records with the scale factor of 60% (60% AC156 input motion,  $S_{DS} = 0.3g$ ) and 200% (200% AC156 input motion,  $S_{DS} = 1.0g$ ) were applied to test specimens and the important information were provided in [Table 3](#).

This study assumed that the specimens were attached to the top floor of the structures. Therefore, the story height ratio was set to 1.0. [Fig. 7](#) shows input acceleration time-history, its elastic response spectrum for damping value of 5%, namely the test response spectrum (TRS), the RRS corresponding to  $S_{DS} = 1.0g$  and the RRS scaled to 90 and 130% ( $A_{FLX-H} = 1.6g$ ,  $A_{RIG-H} = 1.2g$ ,  $A_{FLX-V} = 0.67g$ , and  $A_{RIG-V} = 0.27g$ ). This input acceleration time-history was generated by engineers of the Earthquake Disaster Prevention Research Center of Pusan National University. The figure clearly shows that the input acceleration time history selected to match the ICC-ES AC156 requirements [14]. [Fig. 8](#) presents the correlation coefficient or each direction of the input acceleration time-history for the RRS corresponding to  $S_{DS}$  equal to 1.0g. The maximum cross-correlation function coefficient for the XY, YZ, and ZX planes are 0.15, 0.113, and 0.123, respectively. These values are all less than 0.3, satisfying the IEEE Std. 344 criteria [23] for the statistical independence of ground motions. This input acceleration time history was then scaled to match a level of the target spectrum corresponding to  $S_{DS} = 0.3g$ .

In addition, resonance frequency search tests (Test 2, Test 3 and Test 4) were conducted to determine the fundamental frequencies and dynamic characteristics of the specimens. The tests were conducted in three independent and non-simultaneous directions, corresponding to the X, Y, and Z directions of the shaking table. According to FEMA 461 [15], the input motion was single-axis sinusoidal sweeping at a rate of two octaves/min. It was performed consecutively within the frequency range of 1.0–50 Hz, corresponding to each orthogonal major axis.

#### 4. Test results and discussion

##### 4.1. Fundamental frequency of the specimens

After the sine sweep vibration test was completed, a visual assessment was performed to ensure that no visible damage had occurred to the specimens. By using the frequency domain transfer function technique, it was possible to calculate the fundamental frequencies. The transfer function of a constant linear system is a frequency response function that characterizes the dynamic behavior of the system under consideration. It is the relationship between the Fourier transformation responses of the output signals (A2, A3, A4, and A5) and the Fourier transformation response of the input signal (A1) acquired from the accelerometer data mounted at various locations throughout the system. The raw experimental data were evaluated using a program written in MATLAB version R2020a [24], which is used to analyze the results.

The transfer function charts are shown in [Fig. 9](#). The fundamental frequency of the specimens and the steel frame results are shown in [Table 4](#). The results of the tests show that the fundamental frequencies are between 8.25 and 19.50 Hz. For the steel frame, the fundamental frequency in the X and Y directions obtained in all tests was essentially identical at accelerometer points A3 and A5, which were put on the T-beam and top of the column, respectively. These investigations were unable to estimate the fundamental frequency in the Z direction of the frame.

By comparing the fundamental frequency of the proposed system to that of the existing system. The addition of the pulley increased the fundamental frequencies of the system by 12%, 2.63%, and 12.12% in each of the three directions X, Y, and Z, respectively. Thus, it can be concluded that the addition of the pulley increases the stiffness of the system, particularly in the X and Z directions.

##### 4.2. Visual inspection

Prior to and following testing, the specimens of the pulley wireway system and the existing system were visually inspected for deformation and damage. After visual inspection, a series of shaking table tests found no significant structural failure and no significant damage at the connections of the specimens.

None of the specimens toppled over or collapsed in general. Lights continued to work smoothly and frequently throughout the system. Therefore, it was demonstrated that the pulley wireway system specimens operate efficiently during an earthquake in South Korea, which is located in a moderate-seismic zone, through a series of trials by triaxial shaking satisfying the AC156.

##### 4.3. Steel frame acceleration response

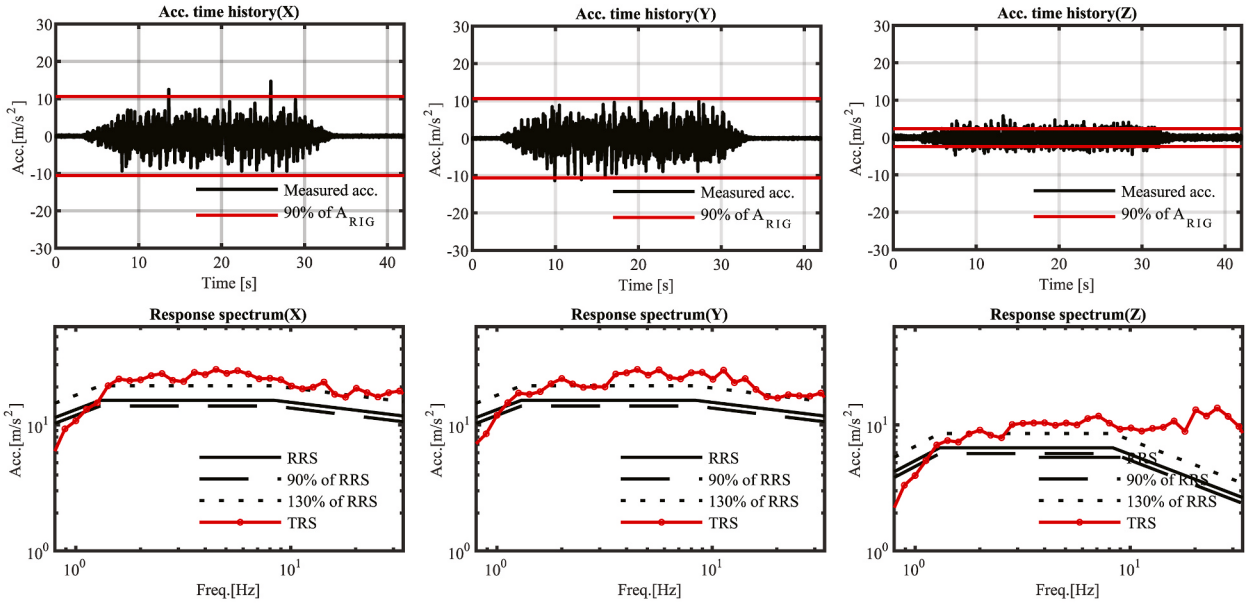
The acceleration response of the frame during Test 1 and Test 5 in the time domain is shown in [Fig. 10](#). The variation in the frame

**Table 3**

Test plan, input, test protocol and peak ground acceleration.

Test No.	Input motion	$S_{DS}$ (g)	Scaling factor(%)	Input PGA(g)		
				X-Dir	Y-Dir	Z-Dir
1	60% AC156 input motion	0.30	60	0.46	0.43	0.17
2	Single-axis sinusoidal sweeping from 1 to 50 Hz (2 octave/min)			0.1 ± 0.05		
3					0.1 ± 0.05	
4						0.1 ± 0.05
5	200% AC156 input motion	1.00	200	1.52	1.13	0.46

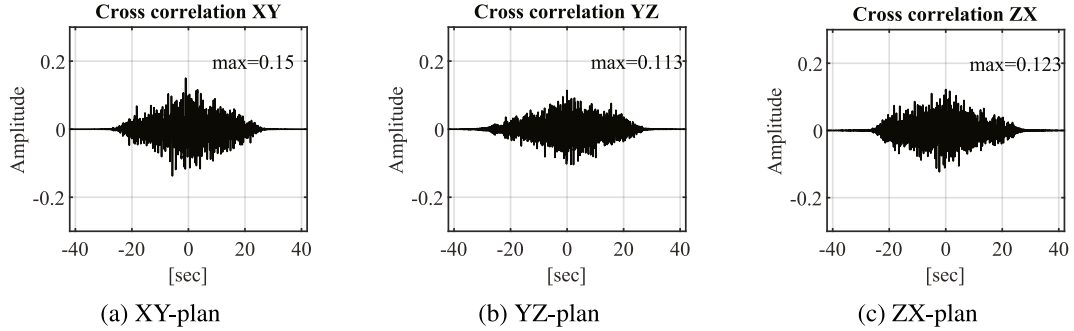
PGA: Peak ground acceleration.



(a) X-Direction

(b) Y-Direction

(c) Z-Direction

Fig. 7. Input acceleration time history corresponding to  $S_{DS} = 1.0g$ , TRS, RRS, upper and lower matching limits.Fig. 8. Correlation coefficient of input motion corresponding to  $S_{DS} = 1.0g$  (200% AC156).

response acceleration with height was determined using the graph superposition approach. The acceleration response values obtained from accelerometers A1, A3, and A5 are represented in cyan, black, and red, respectively. As can be seen, the area of cyan is the smallest in all experiments in the X and Y directions, followed by red and black. Therefore, in the X and Y directions, the acceleration response of the frame is proportional to its height. By comparison, the Z direction response acceleration value is insensitive to the height of the frame.

#### 4.4. Evaluating the efficiency of the pulley

##### 4.4.1. The capacity of reducing the displacement response

The static LVDT data were used to estimate the displacement response of the test specimen in the X-direction. The results indicate that adding the pulley has no influence on the X-direction displacements of the system.

##### 4.4.2. The capacity of reducing the acceleration response

**Peak acceleration response:** The peak acceleration responses of the test specimens in the X, Y, and Z directions are summarized in Table 5. The pulley has the effect of reducing the peak acceleration of the pulley wireway system specimen in the X and Y directions by 10.06% and 10.70%, respectively, and raising it by 68.48% in the Z direction, when the input motion is 60% AC156. When a 200% AC156 input motion is used, the peak response acceleration of the pulley wireway system exceeds that of the existing system in the X direction by up to 110.56% and by 7.48% and 2.04% in the Y and Z directions, respectively. As a result, the proposed system has a higher peak response acceleration, particularly in the X and Z directions, when compared to the existing system. Because of this, when the input motion is a small magnitude and a strong magnitude, the pulley is inefficient in terms of minimizing the peak response acceleration in the time domain.

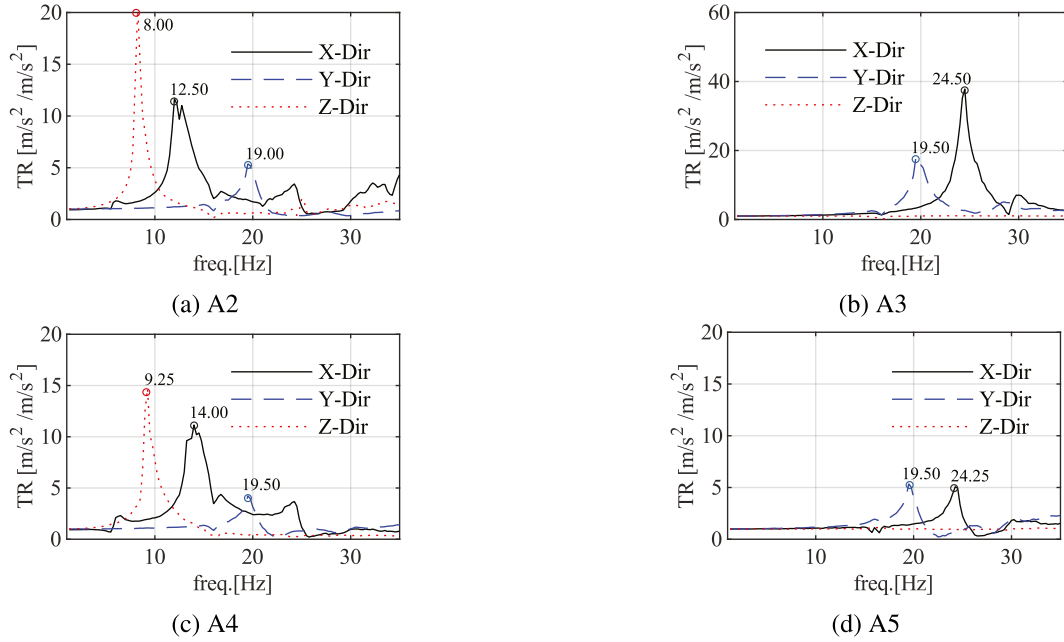


**Fig. 9.** The transfer function plot of resonance frequency search test at accelerometer A2, A3, A4 and A5.

**Table 4**  
Resonance frequencies results.

Specimen	Location	Fundamental frequency (Hz)			Remark
		X-Dir	Y-Dir	Z-Dir	
Existing system	A2	12.50	19.00	8.25	<a href="#">Fig. 9a</a>
Top of the T-beam	A3	24.50	19.50	N/A	<a href="#">Fig. 9b</a>
Pulley wireway system	A4	14.00	19.50	9.25	<a href="#">Fig. 9c</a>
Top of the column	A5	24.25	19.50	N/A	<a href="#">Fig. 9d</a>

**Acceleration response:** To determine the effect of adding the pulley to the proposed system on minimizing the acceleration response, the graph superposition approach was utilized. On the same graph, the acceleration responses of the existing system and the pulley wireway system are plotted in the time domain. As the plot area increases, the acceleration response increases.

As shown in [Fig. 11](#), the purple indicates the acceleration response of the pulley type wireway system specimen, whereas the green represents the acceleration response of the existing system in Test 1 and Test 5. According to [Fig. 11a](#), [b](#), and [11c](#) when the two specimens subjected to the 60% AC156 input motion are compared, it is clear that the acceleration response of the pulley wireway system specimen is slightly less in the X and Y directions and slightly larger in the Z direction than the acceleration response of the existing system specimen. As shown in [Fig. 11d](#), [e](#), and [Fig. 11f](#), when the input motion is 200% of the AC156, the acceleration response of the pulley wireway system is significantly smaller than the acceleration response of the existing system specimen in all directions. Based on these results, it was demonstrated that the pulley is effective at reducing the acceleration response, and its effectiveness increases proportionately with the magnitude of the earthquake.

#### 4.4.3. The capacity of reducing the peak resonant oscillation

The behavior of the proposed system and the existing system needs to be carefully considered when resonance occurs during earthquakes. Thus, a comprehensive and detailed investigation in the frequency domain was carried out to demonstrate the effectiveness of the pulley in dissipating earthquake energy in earthquakes of varying magnitudes. The acceleration spectral density (ASD) and acceleration root mean square (ARMS) functions were used to evaluate and compare the dynamic behavior of the pulley wireway system and an existing system specimen.

The ASD plot depicts the acceleration response distribution for each frequency measured using the shaking table experiment. An approach for calculating the ASD functions of the measured data is Welch's method [\[25,26\]](#). Denote the  $m$ th windowed, zero-padded frame from the signal  $x$  as follows:

$$x_m(n) \triangleq \omega(n)x(n + mR) \quad (8)$$

$n = 0, 1, \dots, M - 1, m = 0, 1, \dots, K - 1$  where  $R$  is defined as the window hop size and let  $K$  denote the number of available frames. Then, the periodogram of the  $m$ th block is given by:

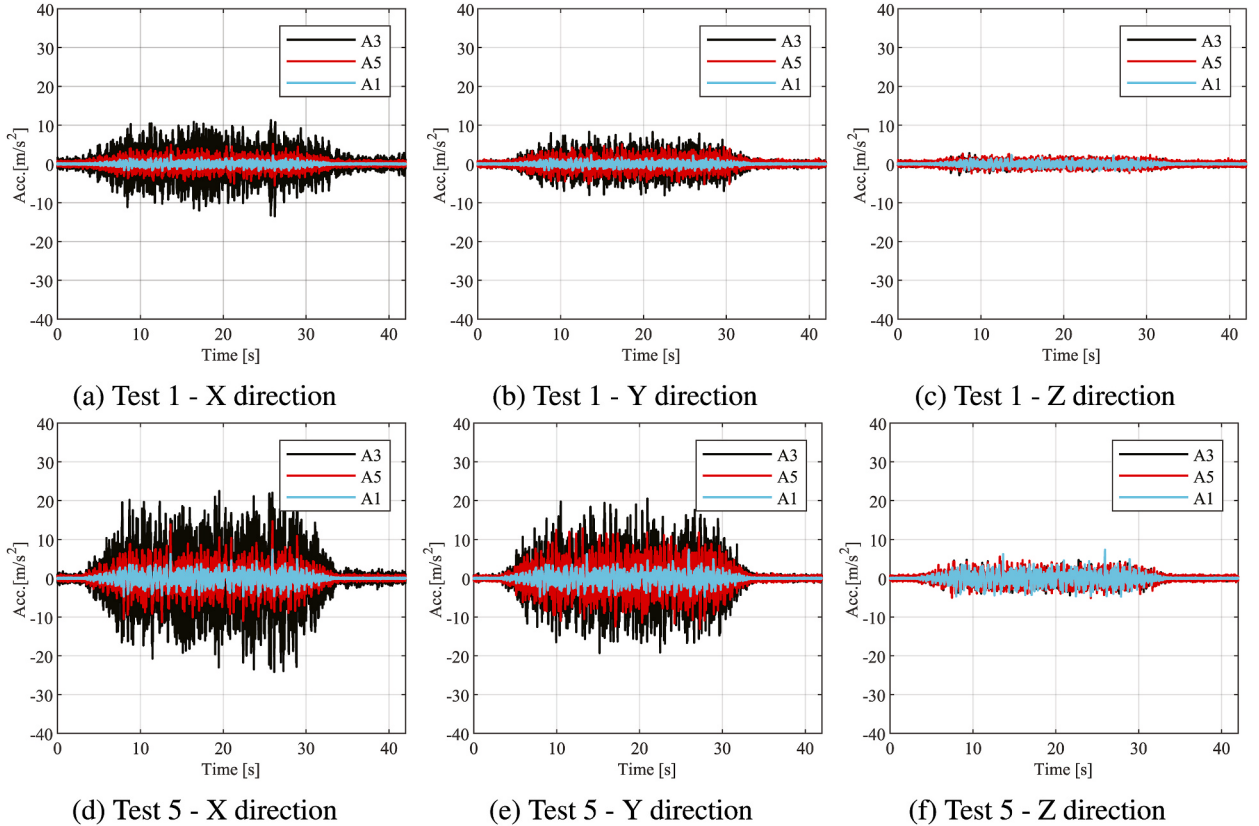


Fig. 10. Acceleration response-time history of the frame in Test 1 and Test 5.

**Table 5**  
Peak response acceleration at the middle of the specimens.

Test no.	Specimen under test	$S_{DS}$ (g)	Peak response acceleration (m/s <sup>2</sup> )		
			Middle position		
			X-Dir	Y-Dir	Z-Dir
1	Existing system	0.3	17.4286	9.0443	9.7192
	Pulley wireway system		15.6746	8.0765	16.3719
5	Existing system	1	46.4635	44.1296	64.4678
	Pulley wireway system		97.8332	47.4297	65.7828

$$P_{x_m,M}(\omega_k) = \frac{1}{M} |\text{FFT}_{N,k}(x_m)|^2 \triangleq \frac{1}{M} \left| \sum_{n=0}^{N-1} x_m(n) e^{-j2\pi n k/N} \right|^2 \quad (9)$$

As previously noted, the Welch estimate of the power spectral density is as follows:

$$\hat{S}_x^w(\omega_k) \triangleq \frac{1}{K} \sum_{m=0}^{K-1} P_{x_m,M}(\omega_k) \quad (10)$$

In this study, the acceleration spectral density (ASD) represents the average vibration intensity, as a function of the frequency during an earthquake. ASD is measured in  $G^2/\text{Hz}$ . The ASD values of the pulley wireway system and an existing system were calculated in MATLAB 2020a using the Welch's Method and shown in Fig. 12. The input parameters used for the ASD calculation in this study were number of points in each segment ( $M = 1024$ ), number of segments ( $K = 21$ ), segments contain 50% overlap ( $S = 0.5 M$ ), time per segment (2 s), and df (0.5 Hz).

According to Fig. 12, there is a sudden increase in the ASD value in both Test 1 and Test 5 due to resonance occurring in all three X, Y, and Z directions. Table 6 shows the first resonance frequency and corresponding peak value of ASD. The results in this table are consistent with the resonance search test results Table 4. This demonstrates that the results of the experiment are extremely dependable.

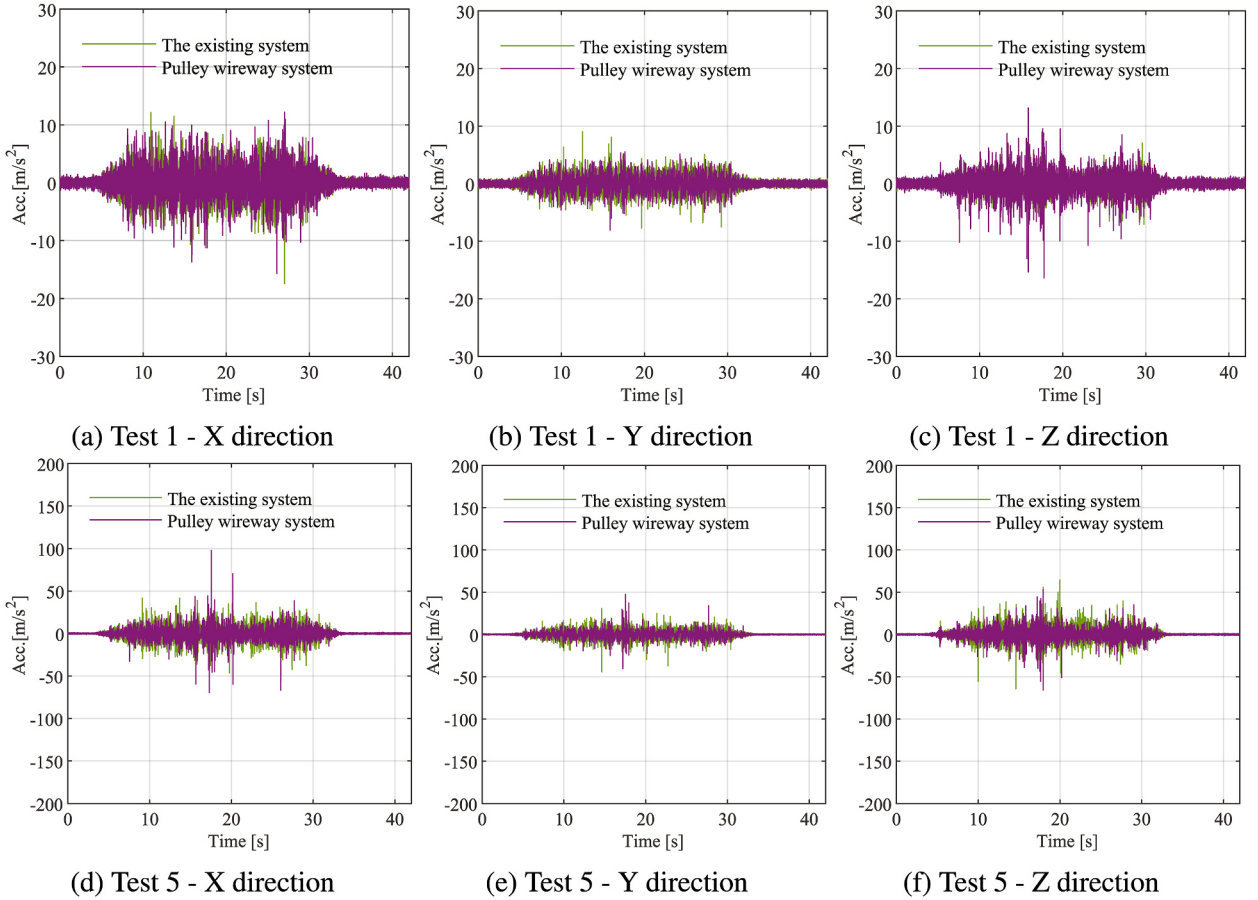


Fig. 11. Acceleration response-time history of Test 1 and Test 5.

As shown in Fig. 12a, b and c, when the motion input is 60% of the AC156, comparing the peak ASD values of the pulley wireway system to those of the existing wireway system clearly shows that the pulley has the effect of reducing the peak ASD values at the resonant frequency in the X and Y directions, which are 30.22% and 33.33%, respectively. In comparison, the ASD value at the resonant frequency in the pulley wireway system is up to 100% more in the Z direction than the ASD value in the existing system. Thus, the pulley reduces the peak oscillation value at the frequency of vibration in the X and Y directions when the system is subjected to low-intensity earthquakes, but it has no effect on lowering the vibration in the Z direction.

According to Fig. 12d, e and f, when the motion input is 200% of the AC156, the pulley is effective in dramatically reducing both the peak ASD values at the resonant frequency in the X, Y, and Z directions by 73.12%, 34.92%, and 70.10%, respectively. Therefore, using a pulley as a friction damper successfully minimizes the maximum oscillation of the system in both the X and Y and Z directions. The efficacy of the pulley is proportional to the magnitude of the earthquake.

#### 4.4.4. The capacity of the earthquake energy dissipation

The root mean square acceleration (ARMS) is a measure of the energy accumulated in a structure as a result of an earthquake. The term “ARMS” refers to the root mean square of the square of the acceleration response during a certain time period (sampling time), which may be computed using Eq. (11) [27]. Here,  $a(t)$  denotes the time-dependent acceleration response;  $t_0$  denotes the start time;  $T_d$  denotes the vibration measurement time, and  $E(T_d)$  denotes the total energy for the period  $T_d$ .

$$ARMS = \frac{E(T_d)}{T_d} = \left[ \frac{1}{T_d} \int_{t_0}^{t_0+T_d} a^2(\tau) d\tau \right]^{1/2} \quad (11)$$

Similarly, temporal ARMS can be defined by replacing  $T_d$  with a small-time interval  $\Delta t$  as follows:

$$ARMS(t) = \left[ \frac{1}{\Delta t} \int_t^{t+\Delta t} a^2(\tau) d\tau \right]^{1/2} \quad (12)$$

for  $\Delta t \rightarrow 0$

In the frequency domain, the ARMS is defined as the square root of the area under the ASD curve. The area under the ASD curve of

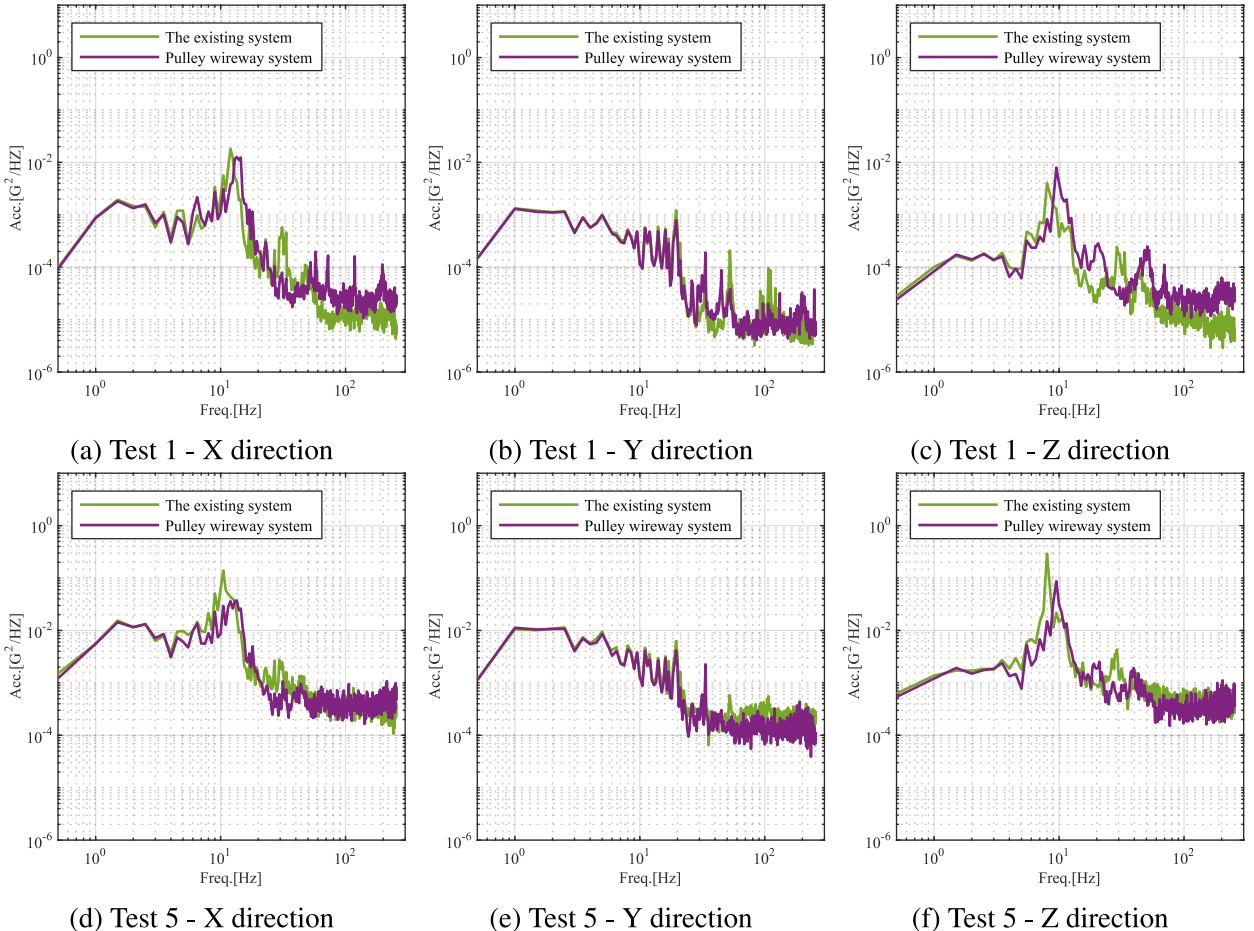


Fig. 12. ASD plots of tri-axial vibration of Test 1 and Test 5.

**Table 6**  
First resonant peak frequency and corresponding ASD value.

Test no.	Specimen under test	$S_{DS}$ (g)	Middle position					
			X-Dir		Y-Dir		Z-Dir	
			ASD ( $G^2/Hz$ )	Freq. (Hz)	ASD ( $G^2/Hz$ )	Freq. (Hz)	ASD ( $G^2/Hz$ )	Freq. (Hz)
1	Existing system	0.30	0.0182	12.00	0.0013	1.00	0.0040	8.00
	Pulley wireway system	0.30	0.0127	13.50	0.0013	1.00	0.0080	9.50
5	Existing system	1.00	0.1388	10.50	0.0114	2.50	0.2916	8.00
	Pulley wireway system	1.00	0.0373	13.50	0.0112	1.00	0.0872	9.50

the  $j$ th frequency segment ( $a_j$ ) between the frequencies  $f_{i-1}$  and  $f_i$  corresponds to  $P_{i-1}$  and  $P_i$  [28].

$m$  is the slope of the segment  $j$  between the frequencies  $f_{i-1}$  and  $f_i$ :

$$m = 10 \log \left( \frac{P_i}{P_{i-1}} \right) \frac{\log(2)}{\log \left( \frac{f_i}{f_{i-1}} \right)} \quad (13)$$

for  $m \neq -10 \log(2)$ :

$$a_{f_i,j} = 10 \log(2) \frac{P_i}{10 \log(2) + m} \left[ f_i - f_{i-1} \left( \frac{f_{i-1}}{f_i} \right)^{m/10 \log(2)} \right] \quad (14)$$

for  $m = -10 \log(2)$ :

$$a_{f_i,j} = P_{i-1} f_{i-1} \ln \left( \frac{f_i}{f_{i-1}} \right) \quad (15)$$

The ARMS value at  $j$ th frequency segment:

$$ARMS_j = \sqrt{a_j} \quad (16)$$

The overall ARMS level at  $j$ th at frequency  $f_i$  is then:

$$ARMS_{f_i} = \sum_{m=0}^j a_m \quad (17)$$

In the frequency domain, the ARMS values of the vibration response are determined using cumulative distribution functions (CDFs). The CDF curves in the X, Y, and Z directions are shown in Fig. 13 for the pulley wireway system specimen and existing system subjected to a 60% AC156 input motion and 200% AC156 input motion.

The CDF curves for two specimens are divided into three ranges: low frequency range (0–8 Hz), resonance frequency range (8–14 Hz), and high frequency range ( $>14$  Hz). The CDF curves of the two specimens are nearly consistent in the low frequency range (0–8 Hz), demonstrating that the pulley is ineffective in reducing the earthquake energy in this range. Similarly, the CDF curves of the two specimens are almost identical in the high frequency region for the 60% AC156 input motion and parallel for the 200% AC156 input motion. This demonstrates that the pulley is inefficient at reducing the energy at high frequencies ( $>14$  Hz). The CDF of the pulley wireway system specimen has a lower slope than the CDF of the existing system specimen in the resonant frequency range (8–14 Hz) for both the 60% and 200% AC156 input motions. Additionally, comparing the position curves of the two specimens reveals that the pulley wireway system specimen has a lower seismic energy than the existing system specimen for the 200% AC156 input motion. Thus, the pulley provides two important functions: it dissipates the seismic energy in the resonant frequency range and spreads the abrupt rise in earthquake energy caused by the resonance over a wider frequency range.

The overall ARMS is the value at the end of the CDF curve presented in Table 7. When the system was subjected to a 60% AC156 input motion, a comparison of the overall ARMS of the specimens showed that the pulley effectively reduced the earthquake energy by 3.16% in the Y direction. In comparison, the pulley increased the energy and magnitude of the earthquake by 8.22% and 35.36%, respectively, in the X and Z directions. As a result, the pulley is ineffective at dissipating seismic energy at low seismic magnitudes.

When the system was subjected to the 200% AC156 input motion, the pulley significantly reduced the earthquake energy in all three directions (X, Y, and Z) by 13.9%, 11.11%, and 18.14%, respectively. As a result, the pulley wireway system is successful at dissipating earthquake energy in a proportional manner to the magnitude of the earthquake.

Table 8 presents the overall ARMS of the acceleration response at the base, top of the T-beam and top of the column in the shaking table test in Test 1 and Test 5. From this result, the overall ARMS of the frame at the mounting position of each specimen is derived using the interpolation approach based on the mounting height of the systems, indicated in Table 9. It is worth noting that the magnitude of the earthquake acceleration acting on the system is not the same in each direction. Thus, the “Energy Transfer Ratio” (ETR) was developed to determine the ratio of the energy transmission in each direction from the frame to the system. It is the ratio of the ARMS of the system in each direction to the ARMS of the system at the hanging position of the frame.

The ETR coefficients in the X, Y and Z directions of pulley wireway system specimen subjected to the 60% and 200% AC156 input motions are depicted in Fig. 14. As can be seen, for the ETR value of the system in the Z direction, the ETR value is highest at both 60% and 200% AC156 input motion. Furthermore, the ETR coefficient increased the most in the Z direction, increasing by 69.384% when the seismic acceleration ETR increased from 60% to 200% AC156, followed by the directions Y and X, which increased by 18.18% and 6.49%, respectively, when the seismic acceleration ETR increased. As a result, the efficiency of the system in dissipating the seismic energy in the Z direction is at its lowest. Therefore, additional seismic energy dissipation mechanisms in the Z direction are required for the pulley wireway system, which will be considered in further studies.

## 5. Conclusion

This study presents the results of tri-axial shaking table tests conducted on a proposed pulley wireway system aimed at increasing the earthquake resistance of existing lighting support structures. The input acceleration time histories were created artificially using the ICC-ES AC156 code and varied in amplitude. Throughout the test campaign, five shaking table tests were conducted, and two specimens were tested. The seismic performance of the pulley wireway system was evaluated and compared with an existing structural support system. The following primary conclusions may be drawn from the test findings.

- After visual inspection, a series of shaking table tests found no significant structural failure and no significant damage at the connections of the specimens. It was demonstrated that the pulley wireway system specimens operate efficiently during an earthquake in Korea, which is located in a moderate-seismic zone, through a series of trials on tri-axial shaking satisfying the AC156 standard.
- The additional pulley increases the fundamental frequency of the system by 12.00%, 2.63%, and 12.12% in the X, Y, and Z directions.
- The pulley provides a high capacity for energy dissipation, which increases with the magnitude of the earthquake. Particularly, when the system was subjected to a 200% AC156 input motion, adding a pulley lowered the seismic energy of the system by 13.90%, 11.11%, and 18.13% in the X, Y, and Z directions. However, the experiment results revealed that adding a pulley has no effect on reducing the displacement of the system in the lateral direction.

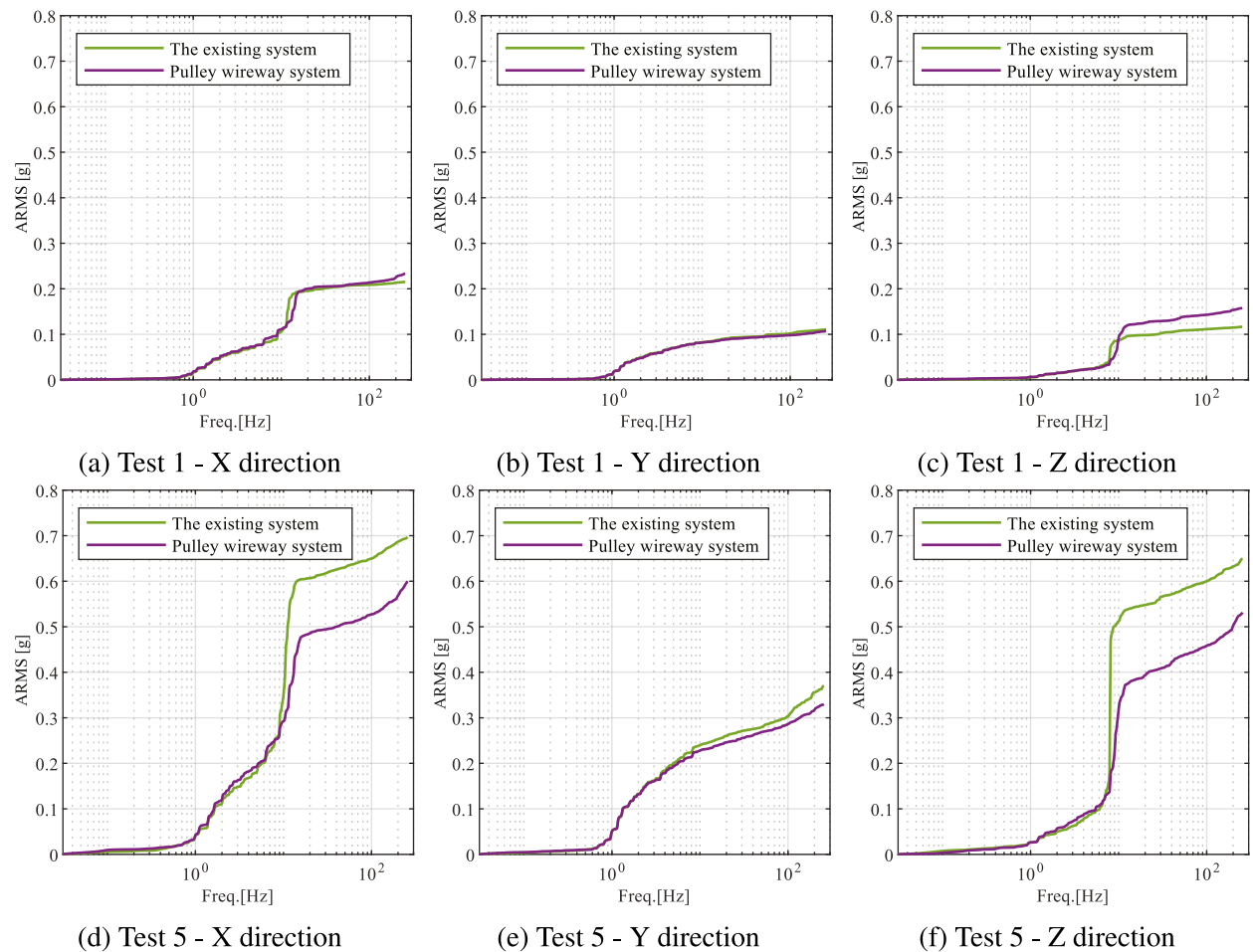


Fig. 13. Cumulative acceleration root mean square plots of tri-axial vibration of Test 1 and Test 5.

**Table 7**

Overall ARMS values of the existing system and pulley wireway system.

Test no.	Specimen under test	$S_{ps}$ (g)	Overall RMS		
			Middle position		
			X-Dir	Y-Dir	Z-Dir
1	Existing system	0.3	0.2153	0.1107	0.1165
	Pulley wireway system		0.233	0.1072	0.1577
5	Existing system	1	0.697	0.3708	0.649
	Pulley wireway system		0.6001	0.3296	0.5313

**Table 8**

Overall ARMS of acceleration response of the frame at accelerometers A1, A3 and A5.

Test no.	Overall ARMS A1,A3,A5 (g)	A1(z = 0 m)			A5(z = 1.645 m)			A3(z = 2.717 m)		
		X-Dir	Y-Dir	Z-Dir	X-Dir	Y-Dir	Z-Dir	X-Dir	Y-Dir	Z-Dir
1	0.090	0.088	0.056	0.116	0.118	0.060	0.294	0.200	0.053	
5	0.244	0.251	0.112	0.266	0.295	0.118	0.582	0.479	0.110	

**Table 9**

Overall ARMS of the frame at mounting position of specimens.

Test no.	Specimen under test	$S_{DS}$ (g)	Overall ARMS (g)		
			Mounting position		
			X-Dir	Y-Dir	Z-Dir
1	Existing system	0.30	0.1068	0.1075	0.0583
	Pulley wireway system		0.1068	0.1075	0.0583
5	Existing system	1.00	0.2583	0.2796	0.1159
	Pulley wireway system		0.2583	0.2796	0.1159

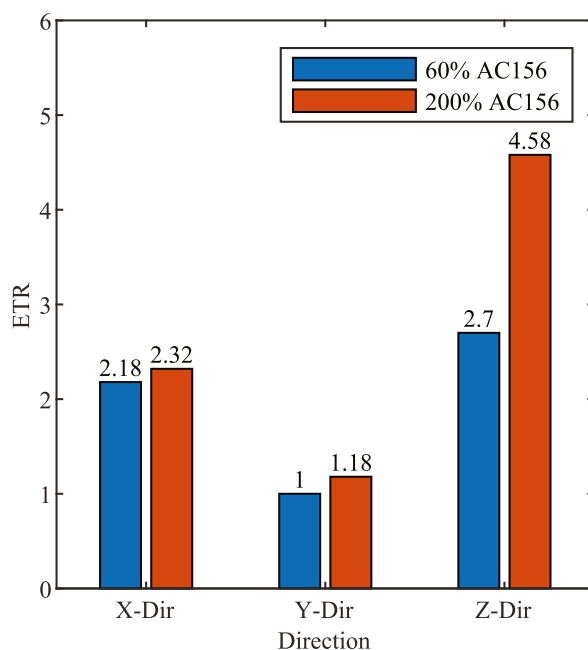


Fig. 14. Energy transmission ratio plots of pulley wireway system specimen.

- The analysis of the system behavior when resonance occurs revealed that using a pulley as a friction damper has the ability to significantly minimize the peak oscillation of the system. The magnitude of the reduction is proportional to the magnitude of the earthquake that the system experienced. In particular, the peak oscillation of the system with the pulleys was reduced by up to 73%, 34.92% and 70.1% in the X, Y, and Z directions, respectively, when compared to the existing system under a 200% AC156 input motion. Furthermore, the pulley has the effect of spreading the abrupt rise in earthquake energy caused by the resonance over a wider frequency range.
- The results of the “Energy transmission ratio” investigation revealed that the ETR in the Z direction accounted for the greatest proportion of the total seismic energy of the specimen. As a result, additional seismic energy dissipation mechanisms in the Z direction are required for the pulley wireway system, which will be considered in further studies.

The pulley friction damper and pulley wireway system were invented to increase the survival of lighting systems during an earthquake, as stated in this study. The seismic performance of the pulley wireway system when connected to several components in the main structure such as the walls, beams, columns, and floors needs further investigation. To augment these findings, the influence of mechanical factors such as friction coefficients, cable pretension, and spring compression force should be investigated. Additionally, additional experimental testing is planned to evaluate the seismic performance of full-scale pulley wireway system specimens ranging in length from five to 50 m.

#### CRediT authorship contribution statement

**Han V. Tran:** Conceptualization, Methodology, Formal analysis, Data collection and analysis, Writing - Original draft preparation, Writing - Reviewing and Editing. **Sung Chan Kim:** Writing – Reviewing and Editing, Formal analysis. **Jiuk Shin:** Writing – Reviewing and Editing, Formal analysis. **Kihak Lee:** Resources, Formal analysis, Writing - Reviewing and Editing, Supervision, Project administration.

## Declaration of competing interest

The authors declare the following financial interests/personal relationships which may be considered as potential competing interests: Kihak Lee reports financial support was provided by Sehong Inc, Ltd and supported by National Research Foundation of Korea (NRF-2020R1A2C2007195).

## Acknowledgements

This research is the projects funded by Sehong Inc. Ltd in 2020. Also this research was supported by National Research Foundation of Korea(NRF-2020R1A2C2007195).

## References

- [1] R. Villaverde, Seismic design of secondary structures: state of the art, *J. Struct. Eng.* 123 (8) (1997) 1011–1019.
- [2] C.A. Kircher, It makes dollars and sense to improve nonstructural system performance, in: *PROC ATC 29-2 SEMINAR ON SEISMIC DESIGN, PERFORMANCE, AND RETROFIT OF ...*, 2003.
- [3] A. Filiatrault, T. Sullivan, Performance-based seismic design of nonstructural building components: the next frontier of earthquake engineering, *Earthq. Eng. Eng. Vib.* 13 (1) (2014) 17–46.
- [4] E. FEMA, Reducing the Risks of Nonstructural Earthquake Damage, Practical Guide, January.
- [5] D. Ding, C. Arnold, H. Lagorio, S. Tobriner, S. Rihal, R. Mangum, G. Hezmalhalch, M. Green, A. Watson, D. Mah, et al., Architecture, building contents, and building systems, *Earthq. Spectra* 6 (S1) (1990) 339–377.
- [6] L. Qi, M. Kurata, Y. Ikeda, K. Kunitomo, M. Takaoka, Seismic evaluation of two-elevation ceiling system by shake table tests, *Earthq. Eng. Struct. Dynam.* 50 (4) (2021) 1147–1166.
- [7] R. Villaverde, Methods to assess the seismic collapse capacity of building structures: state of the art, *J. Struct. Eng.* 133 (1) (2007) 57–66.
- [8] K.A. Institute, Pohang Earthquake Damage Survey Report, Korea Architectural Institute, Seoul, Korea, 2018.
- [9] H.H. Hwang, J.-R. Huo, Seismic fragility analysis of electric substation equipment and structures, *Probabilist. Eng. Mech.* 13 (2) (1998) 107–116.
- [10] K. Porter, G. Johnson, R. Sheppard, R. Bachman, Fragility of mechanical, electrical, and plumbing equipment, *Earthq. Spectra* 26 (2) (2010) 451–472.
- [11] D. Wang, J. Dai, Z. Qu, X. Ning, Shake table tests of suspended ceilings to simulate the observed damage in the m s 7.0 lushan earthquake, China, *Earthq. Eng. Eng. Vib.* 15 (2) (2016) 239–249.
- [12] H. Son, S. Park, B.-G. Jeon, W.-Y. Jung, J. Choi, B.-S. Ju, Seismic qualification of electrical cabinet using high-fidelity simulation under high frequency earthquakes, *Sustainability* 12 (19) (2020) 8048.
- [13] N.H. Dinh, S.-J. Lee, J.-Y. Kim, K.-K. Choi, Study on seismic performance of a mold transformer through shaking table tests, *Appl. Sci.* 10 (1) (2020) 361.
- [14] E. ICC, Ac156 Acceptance Criteria for Seismic Certification by Shake-Table Testing of Nonstructural Components, International Code Council Evaluation Service, Country Club Hills, IL.
- [15] F. FEMA, 461-interim Protocols for Determining Seismic Performance Characteristics of Structural and Nonstructural Components through Laboratory Testing, Federal Emergency Management Agency (Fema), Document No, Redwood City, CA, 2007.
- [16] H. Usabiaga, M. Ezkurra, M. Madoz, J. Pagalday, Experimental test for measuring the normal and tangential line contact pressure between wire rope and sheaves, *Exp. Tech.* 32 (5) (2008) 34–43.
- [17] V.A. Lubarda, Determination of the belt force before the gross slip, *Mech. Mach. Theor.* 83 (2015) 31–37.
- [18] L. Euler, Remarques sur l'effet du frottement dans l'équilibre, *Mémoires de l'académie des sciences de Berlin*, 1769, pp. 265–278.
- [19] Shake-table Testing Method for Seismic Performance Evaluation of Suspended Ceiling, Standard, Korea Construction Engineering Development Collaboratory Management Institute, Gyeonggi-do, ROK, Feb. 2021.
- [20] S.-C. Jun, C.-H. Lee, C.-J. Bae, K.-J. Lee, Shake-table seismic performance evaluation of direct-and indirect-hung suspended ceiling systems, *J. Earthq. Eng.* (2020) 1–19.
- [21] H.-J. Kim, D.-H. Shin, Shake table test program of cold-formed steel in-plane partition walls, in: *Structures*, vol. 30, Elsevier, 2021, pp. 503–517.
- [22] KCSC, Seismic Design Code of Buildings (kds 41 17 00), Sejong, Korea: Ministry of Land, Infrastructure and Transport.
- [23] I. 344, Ieee Standard for Seismic Qualification of Equipment for Nuclear Power Generating Stations, 2013.
- [24] MATLAB, Version 9.8.0 (R2020a), The MathWorks Inc., Natick, Massachusetts, 2020.
- [25] P. Welch, The use of fast fourier transform for the estimation of power spectra: a method based on time averaging over short, modified periodograms, *IEEE Trans. Audio Electroacoust.* 15 (2) (1967) 70–73.
- [26] O. Solomon Jr., Psd computations using welch's method, in: *NASA STI/Recon Technical Report N 92*, 1991, 23584.
- [27] G. Housner, P.C. Jennings, Generation of artificial earthquakes, *J. Eng. Mech. Div.* 90 (1) (1964) 113–150.
- [28] R. Simmons, Calculating grms (root-mean-square acceleration), URL, <https://femci.gsfc.nasa.gov/random/randomgrms.html>, 1997.